DOA-based Localization Using Deep Learning for Wireless Seismic Acquisition

Kabiru N. Aliyu
Electrical Engineering Department and Center for Communication Systems and Sensing, King Fahd University of Petroleum and Minerals (KFUPM), Dhahran 31261, Saudi Arabia

Saleh A. Alawsh
Electrical Engineering Department and Center for Communication Systems and Sensing, King Fahd University of Petroleum and Minerals (KFUPM), Dhahran 31261, Saudi Arabia

Ali H. Muqaibel (muqaibel@kfupm.edu.sa)
Electrical Engineering Department and Center for Communication Systems and Sensing, King Fahd University of Petroleum and Minerals (KFUPM), Dhahran 31261, Saudi Arabia

Suhail I. Al-Dharrab
Electrical Engineering Department and Center for Communication Systems and Sensing, King Fahd University of Petroleum and Minerals (KFUPM)

Wessam Mesbah
Electrical Engineering Department and Center for Communication Systems and Sensing, King Fahd University of Petroleum and Minerals (KFUPM), Dhahran 31261, Saudi Arabia

Varun A. Reddy
School of Electrical and Computer Engineering, Georgia Institute of Technology, Atlanta, GA 30332, USA

Ahmad Bazzi
CEVA Les Bureaux Green Side 5, Bat 6 400, avenue Roumanille 06410 Biot, Sophia Antipolis, France

Gordon L. Stüber
School of Electrical and Computer Engineering, Georgia Institute of Technology, Atlanta, GA 30332, USA

Research Article

Keywords: Deep neural network, DOA estimation, Least square location estimator, Wireless gateway node, Wireless geophone, Wireless seismic acquisition

Posted Date: September 28th, 2021

DOI: https://doi.org/10.21203/rs.3.rs-925575/v1

DOA-based Localization Using Deep Learning for Wireless Seismic Acquisition

Kabiru N. Aliyu[1], Saleh A. Alawsh[1] (Member, IEEE), Ali H. Muqaibel[1,*] (Senior Member, IEEE), Suhail I. Al-Dharrab[1] (Member, IEEE), Wessam Mesbah[1] (Senior Member, IEEE), Varun A. Reddy[2] (Graduate Student Member, IEEE), Ahmad Bazzi[3], and Gordon L. Stüber[2] (Fellow, IEEE)

[1]Electrical Engineering Department and Center for Communication Systems and Sensing, King Fahd University of Petroleum and Minerals (KFUPM), Dhahran 31261, Saudi Arabia
(e-mail: g201705110, salawsh, muqaibel*, suhaild, mesbahw@kfupm.edu.sa)
[2]School of Electrical and Computer Engineering, Georgia Institute of Technology, Atlanta, GA 30332, USA
(e-mail: varun.reddy, stuber @gatech.edu)
[3]CEVA Les Bureaux Green Side 5, Bat 6 400, avenue Roumanille 06410 Biot, Sophia Antipolis, France
(e-mail: ahmad.bazzi@ceva-dsp.com)

*Corresponding author: Ali H. Muqaibel (muqaibel@kfupm.edu.sa)

This work is supported by the Center for Energy and Geo Processing at Georgia Institute of Technology and King Fahd University of Petroleum and Minerals (KFUPM), under grant number GTEC1601.

***Abstract*—**Oil and gas companies consider transforming conventional cable-based seismic acquisition to wireless acquisition as a promising step for cost and weight reduction in reservoir exploration. Wireless seismic acquisition requires large number of wireless geophone (WG) sensors to be deployed in the field. The locations of the WG sensors must be known when processing the collected data. The application of direction of arrival (DOA) estimation helps in localizing WGs and improves received signal level through beam steering and interference avoidance. Conventional DOA algorithms require high computational complexity which renders them inefficient for real-time response. In this paper, deep neural network (DNN) is proposed for DOA estimation of WGs at wireless gateway node (WGN) under different channel conditions. The estimated angle and corresponding coordinates of WGNs are used in least square estimation (LSE) to estimate the position of the WGs. The simulation results depict reasonable estimation and position accuracy in real-time.

***Keywords*—** Deep neural network, DOA estimation, Least square location estimator, Wireless gateway node, Wireless geophone, Wireless seismic acquisition

1 Introduction

SEISMIC acquisition is usually carried out by oil and gas, and mineral resources companies for reservoir identification. In seismic exploration, a seismic signal is generated from a localized seismic source, usually a vibroseis truck [1], [2]. The seismic signal is reflected by subsurface discontinuities in the Earth and measured by geophones. Conventional seismic surveys rely on cable-based systems for transmission of the measured signal from the geophone sensors to the storage/processing unit for further investigation. The massive increase in the number of geophone sensors from about 1,000 to 2,000 geophones per square kilometer leads to a great challenge in equipment weight, flexibility and cost [3]. Oil and gas companies foresee wireless transmission of the measured seismic signals to the storage/processing unit as a promising technology. While wireless systems offer an excellent alternative to cable, they come with the challenging task of achieving high data rates and synchronization over the deployed nodes across a widespread area [4], [5]. Real-time acquisition is of vital importance as it enables field engineers to adaptively modify the acquisition parameters and minimize logistical costs [4], [5]. Knowing the direction of arrival (DOA) of the transmitted signal and the position of the transmitter is paramount to geophysical and communication purposes [6], [7], [8].

Different architectures for wireless seismic acquisition have been proposed for proper replacement of the conventional cable-based system [3], [9]–[14]. The authors in [9] introduced star topology with a single wireless gateway node (WGN) to coordinate 1024 wireless geophones (WGs). Reference [11] proposed 1,000 to 2,000 WGs with spacing of 5 m to 30 m. The authors in [12] divided the whole area of acquisition into subnetworks, each subnetwork having ~200 to 300 WGs that are coordinated by a single WGN. For an orthogonal deployment, the spacing between WGs is 20 m to 40 m along the vertical lines and 0.5 km to 1 km along the horizontal lines. In [3] and [13], similar geometries were utilized as in [11] with addition of cluster heads to coordinate the leaf-nodes, i.e. WGs, and the survey area was extended beyond 30 $sq\ km$. An orthogonal geometry was used by [10] and [14], where 4,707 WGs with 30 m interspacing were deployed in 22.5 $sq\ km$ [10]. The authors in [14] used 30 receiver lines (RLs) with 200 m interspacing, where 480 WGs were deployed along each RL with a spacing of 25 m. This comprised a total of 14,400 WGs in 72 $sq\ km$.

Researchers have proposed various communication technologies for data transfer between the nodes. The authors in [9], [15], and [16] used Wi-Fi technology, while [3], [11], [12], and [13] proposed ultra-wide band technology due to its

support for high data rate and precise power emission. Other possible technologies include ZigBee, Bluetooth, multi-band orthogonal frequency division multiplexing (MB-OFDM), impulse-radio ultra-wide band (IR-UWB), in addition to mobile infrastructure for long range communication between the WGNs and the storage/processing unit. TV white space band (IEEE 802.11af standard) which ranges from 50 to 700 MHz was also proposed for communication between the WGs and WGNs [14].

Localization of WGs can be achieved by either using a global positioning system (GPS), or by using localization algorithms to estimate the positions of the WGs in GPS deprived environments. Received signal strength (RSS), time-of-arrival (TOA), time difference-of-arrival (TDOA), and DOA are among the candidate localization techniques. This paper focuses on DOA techniques. Recently, localization using sectorized antenna was proposed in [10]. The trends towards multiple input and multiple output systems (MIMO) suggest that beamforming and DOA techniques will be readily available in future systems. Various DOA algorithms have been proposed for localization. The Capon algorithm was initially applied to MIMO systems in [17]. The authors in [18] presented a comparative analysis of Beamforming, the Capon algorithm, MUSIC, and first-norm singular value decomposition (SVD) for two sources impinging on restricted antenna arrays.

Deep neural networks (DNNs), a type of machine learning with multiple interconnected hidden layers has been applied in different fields like image processing, voice recognition, communications, etc [19], [20], [21]. The learning phase of DNNs involves extensive calculations but concedes low complexity and high resolution in estimation. Efforts have been made to integrate DNNs into direction finding. In [22], an artificial neural network was proposed for up to 4 sources, in 10° resolution, using a 5-element uniform linear array (ULA). A DNN for DOA of two sources with 1° resolution was proposed in [23] and [24]. In [25], DNNs were proposed for direction finding of unmanned aerial vehicles. Furthermore, the authors in [26] and [27] integrated DNNs with massive MIMO. In [28], a convolutional neural network based on supervised learning was used in DOA estimation of acoustic signals.

The locations are important for processing collected seismic data, and ultimately obtaining the seismic images. Given two or more estimated DOAs with coordinates of the receiver, the location of the transmitter can be estimated using a least square estimation (LSE) [29], [30]. In [31], DOA estimation based DNN is proposed for wireless seismic survey. In this paper, DNN is proposed for DOA estimation of WGs at the WGN under different channel conditions. Particularly, the estimated angle and corresponding coordinates of WGNs are used to estimate the position of the WGs. The seismic acquisition area is divided into many uniform regular hexagonal cells. Each cell has one WGN at the center serving many WGs. The cell is further divided into three sectors, where a ULA with a given number of elements is used at the WGN to estimate the DOA of the signals received from each WG. It is assumed that one WG is active at a time in each sector. A DNN algorithm is proposed for DOA estimation of the received signal at each sector. The DOA is used to improve the communication quality to support high data rate capability. The estimated angle and corresponding coordinates of WGNs are used in an LSE [29], [30] to estimate the positions of the WGs. The mean absolute error (MAE) and the empirical cumulative distribution function (CDF) are used for localization error analysis. Simulation results depict reasonable estimation and position accuracy in real-time.

The remainder of this paper is organized as follows. Section 2 covers the proposed wireless seismic architecture, including sensor node distribution, channel model, and DOA estimation formulation for wireless seismic acquisition. Section 3 presents the DNN-based DOA estimation scheme. Section 4 introduces the LSE. Simulation and results are discussed in Section 5. Finally, Section 6 wraps up with concluding remarks.

2 Wireless Seismic Architecture

2.1 Sensor Node Distribution (Hexagonal cells)

To decide on the wireless system architecture, knowledge about the topology of the WGs is needed. An orthogonal geometry was adopted in [14], where RLs and source lines (SLs) are perpendicular to each other, as shown in Fig. 1. The red sparks represent the seismic sources along the SL, the black dots represent the WGs deployed along the RL with interspacing Δx, and triangles are the WGNs. The vertical spacing between the RLs is Δy. Wireless coverage is provided to the whole acquisition field by dividing the area into hexagonal cells. Adjacent cells are assumed to be in a horizontal interval of $3R$, where R is the cell radius. A group of WGs in a single cell are coordinated by a single WGN serving as the base station. The number of required cells $N(R)$, as a function of R, is given in [14] as

$$N(R) = \begin{cases} (2\lceil y_c \rceil + 1)\lfloor x_c \rfloor + \lceil y_c \rceil, & \{x_c\} \leq 1/3 \\ (2\lceil y_c \rceil + 1)\lfloor x_c \rfloor, & \{x_c\} > 1/3 \end{cases} \quad (1)$$

$$y_c = \frac{(Y-1)\Delta y}{\sqrt{3}R}, \quad x_c = \frac{(X-1)\Delta x}{3R} \quad (2)$$

where $\lceil \alpha \rceil, \lfloor \alpha \rfloor$ and $\{\alpha\}$ are ceiling, floor, and fractional part of α. Y is the number of RLs, X is the number of WGs in a single RL, $\lceil y_c \rceil$ is the number cells along a single column of cells, and $2\lceil x_c \rceil$ is the number of cells along a single row of cells. In real life, obstructions in the environment introduce uncertainty to the exact locations of the WGs. This can be modeled as a uniformly random perturbed geometry with separation ranging from 0 to $2m$ in each coordinates [3].

Sectorization is applied to each cell, where a directive ULA with 120^o coverage is employed in every sector. This leads to three sectors at each WGN as shown in Fig. 2. Since directed antennas are used in each sector, the WG within a certain sector will be localized with better accuracy. Note that, the number of WGs and RL in Fig. 1 and Fig. 2 are not drawn to scale.

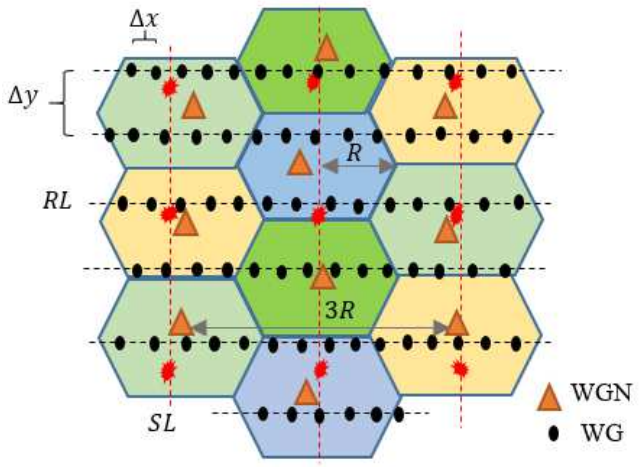

Fig. 1. Orthogonal geometry of wireless seismic architecture.

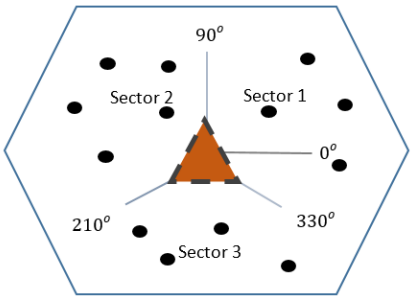

Fig. 2. Single cell with 3 sectors.

2.2 Channel Model

Different environmental factors like free-space loss, scattering, reflection, refraction, or diffraction in the physical channel affect the quality of the signals transmitted from the WGs to the WGNs. To predict the effect of distance, obstacles and other environmental factors on the transmitted signals, reference [32] analyzed both log-distance and log-normal shadowing model for tall and short grassy land environments, while the authors in [33] and [34] performed experimental evaluation of path loss exponent in wireless sensor networks. The log-normal path loss, $\overline{PL}(d)_{dB}$, determines the power loss on the transmitted signal as a function of distance and fading effect; expressed by [32]

$$\overline{PL}(d)_{dB} = \overline{PL}(d_0) + 10\gamma log_{10}\left(\frac{d}{d_0}\right) + X_\sigma \qquad (3)$$

where $\overline{PL}(d_0)$ is the path loss at close reference distance $d_0 = 1\ m$, d is the Euclidian distance between the WG and the WGN, γ is the path loss exponent and X_σ is a log-normal shadowing parameter which is Gaussian random variable with zero mean and variance σ^2. If the distance effect is considered alone in the path loss model, (3) is expressed without X_σ.

2.3 DOA Estimation Formulation in Wireless Seismic Model

Consider the scenario where a single source i.e. WG transmits a narrow band signal $g(t)$, from a distance $\gg 2D^2/\lambda$ (far field assumption) with wavelength λ and D being the aperture size of the array. The transmitted signal is received by an M-element ULA at the WGN, as shown in Fig. 3. The inter-element spacing is $\Delta = \lambda/2$ and the incidence DOA of the received signal is θ. The received signal at the array output, can be expressed as [18]

$$\boldsymbol{x}(t) = \boldsymbol{u}(\theta)g(t) + \boldsymbol{n}(t), \qquad t \in \{1, 2, \dots, T\} \qquad (4)$$

where $\boldsymbol{x}(t) = [x_1(t), x_2(t), \dots, x_M(t)]^T$, $\boldsymbol{n}(t) = [n_1(t), n_2(t), \dots, n_M(t)]^T$ is the additive white Gaussian noise (AWGN) vector, $[.]^T$ is the transpose operation, T is the snapshots, and $\boldsymbol{u}(\theta)$ is the steering vector defined as

$$\boldsymbol{u}(\theta) = \left[1, e^{\frac{j2\pi\Delta sin(\theta)}{\lambda}}, \dots, e^{\frac{j2\pi\Delta(M-1)sin(\theta)}{\lambda}}\right]^T \qquad (5)$$

Since the signal and the noise are uncorrelated, the $M \times M$ correlation matrix of the received signal can be written as

$$\boldsymbol{R_{xx}} = E[\boldsymbol{x}(t)\boldsymbol{x}^H(t)] = \boldsymbol{u}(\theta)\sigma_{gg}^2\boldsymbol{u}^H(\theta) + \sigma_n^2\boldsymbol{I} \qquad (6)$$

where $\sigma_{gg}^2 = E[g(t)g^H(t)]$ is the signal power, σ_n^2 is the common variance of the noise terms, $E[\cdot]$ is the statistical expectation, and $[\cdot]^H$ is a Hermitian operator. The correlation matrix $\boldsymbol{R_{xx}}$ is used as an input to the DNN-based DOA algorithm for estimating DOA of the source.

3 DNN-Based DOA Estimator

This section describes the framework of the DNN and its application for DOA estimation of the received signals at the WGN(s).

3.1 DNN Framework

Fig. 4 shows a conventional single layer neural network with J inputs and an output l. Each input q_j, for $j = 1,2, \dots, J$, is multiplied with analogous weight, $w_{l,j}$, and summed up with a constant bias b_l to produce an output z_l, for $l = 1,2, \dots, L$. An activation function f is a transfer function that controls the J inputs and z_l output of the network through mapping to predict the final output y_l. The output, z_l, and the activation functions can be expressed respectively as [23]

$$z_l = \sum_{j=1}^{J} w_{l,j}q_j + b_l \qquad (7)$$

$$f_{sigmoid}(z_l) = \frac{1}{1+e^{-z_l}}, \quad f_{ReLu}(z_l) = \max(0, z_l) \qquad (8)$$

where $f_{sigmoid}$, f_{ReLu} are the Sigmoid and rectified linear activation functions. The output y_l can be written as [23]

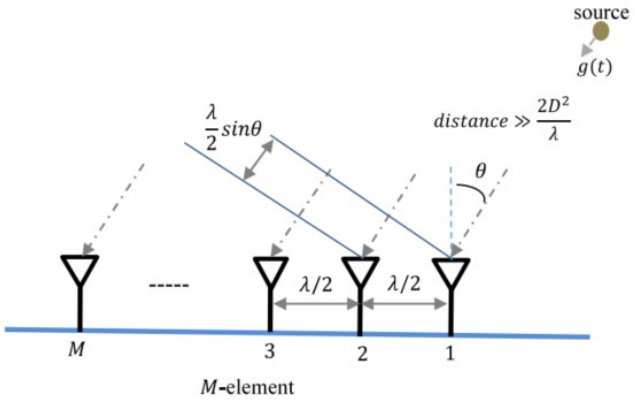

Fig. 3. DOA estimation using ULA.

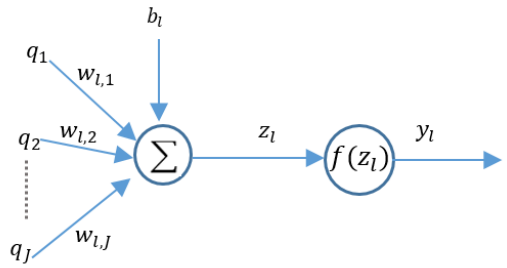

Fig. 4. Single layer neural network.

$$y_l = f(z_l) = f\left(\sum_{j=1}^{J} w_{l,j}q_j + b_l\right) = f\left(\sum_{j=0}^{J} w_{l,j}q_j\right) \quad (9)$$

where the 0^{th} input $q_0 = 1$ is introduced to accommodate for matrix multiplication as in (11) and the equivalent weight is $w_{l,0} = b_l$. It follows that (7) and (9) can be written in vector form as [23]

$$\boldsymbol{y} = \begin{bmatrix} y_1 \\ y_2 \\ \vdots \\ y_L \end{bmatrix} = \begin{bmatrix} f(z_1) \\ f(z_2) \\ \vdots \\ f(z_L) \end{bmatrix} = f(\boldsymbol{z}) \quad (10)$$

$$\boldsymbol{z} = \begin{bmatrix} z_1 \\ z_2 \\ \vdots \\ z_L \end{bmatrix} = \begin{bmatrix} w_{1,0} & w_{1,1} & \cdots & w_{1,J} \\ w_{2,0} & w_{2,1} & \cdots & w_{2,J} \\ \vdots & \vdots & \vdots & \vdots \\ w_{L,0} & w_{L,1} & \cdots & w_{L,J} \end{bmatrix} \begin{bmatrix} 1 \\ q_1 \\ \vdots \\ q_J \end{bmatrix} = \boldsymbol{W}\begin{bmatrix} 1 \\ \boldsymbol{q} \end{bmatrix} \quad (11)$$

3.2 Application of DNN for DOA Estimation

For DOA estimation using DNN, the $M \times M$ correlation matrix $\boldsymbol{R_{xx}}$ of the received signal is used as an input to the DNN. The covariance matrix $\boldsymbol{R_{xx}}$ is a Hermitian matrix in which the diagonal elements are real-valued while the upper and lower triangular parts are complex conjugates of each other. To avoid repetition, the diagonal elements and only the lower or upper entries of $\boldsymbol{R_{xx}}$ are used. The complex values are decomposed and presented as real values arranged in a row vector of length M^2 as [23]

$$\boldsymbol{q} = \left[r_{1,1}, r_{2,2}, \ldots, r_{M,M}, \Re(r_{2,1}), \Im(r_{2,1}), \ldots, \Im(r_{M,M-1})\right]^T \quad (12)$$

where $r_{m,n}$, $\forall\, m,n = 1, \ldots, M$, are the entries of $\boldsymbol{R_{xx}}$ and $\Re(\cdot)$, $\Im(\cdot)$ are the real and imaginary entries.

4 Least Square Location Estimation

For a single WG signal, given two or more DOAs at different WGNs, and the corresponding locations of those WGNs, the location of the WG can be estimated using LSE [35], as described in Fig. 5. Let θ_k be the DOA of the WG to the k^{th} WGN located at $(X_{\mathrm{WGN}_k}, Y_{\mathrm{WGN}_k})$. The position $(X_{\mathrm{WG}}, Y_{\mathrm{WG}})$ of the transmitter can be localized as

$$\frac{\cos\theta_k}{\sin\theta_k} = \frac{X_{\mathrm{WG}} - X_{\mathrm{WGN}_k}}{Y_{\mathrm{WG}} - Y_{\mathrm{WGN}_k}}. \quad (13)$$

This can be expressed as

$$X_{\mathrm{WG}}\sin\theta_k - X_{\mathrm{WGN}_k}\sin\theta_k = Y_{\mathrm{WG}}\cos\theta_k - Y_{\mathrm{WGN}_k}\cos\theta_k \quad (14)$$

Equation (14) for $k = 1,2, \ldots, K$ can be written in matrix form as

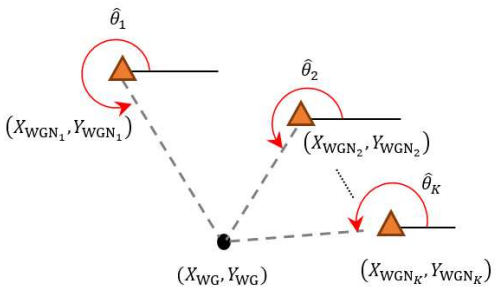

Fig. 5. Descriptive diagram of LSE.

$$\boldsymbol{Ah} = \boldsymbol{v} \quad (15)$$

where K is the number of WGNs used for estimating the WG located at $\boldsymbol{h} = [X_{\mathrm{WG}}, Y_{\mathrm{WG}}]^T$, and the other two variables are

$$\boldsymbol{A} = \begin{bmatrix} \sin\theta_1 & -\cos\theta_1 \\ \sin\theta_2 & -\cos\theta_2 \\ \vdots & \vdots \\ \sin\theta_K & -\cos\theta_K \end{bmatrix}, \quad \boldsymbol{v} = \begin{bmatrix} X_{\mathrm{WGN}_1}\sin\theta_1 - Y_{\mathrm{WGN}_1}\cos\theta_1 \\ X_{\mathrm{WGN}_2}\sin\theta_2 - Y_{\mathrm{WGN}_2}\cos\theta_2 \\ \vdots \\ X_{\mathrm{WGN}_K}\sin\theta_K - Y_{\mathrm{WGN}_K}\cos\theta_K \end{bmatrix} \quad (16)$$

Therefore, the LSE for the unknown location of the WG transmitter is expressed as

$$\hat{\boldsymbol{h}} = (\boldsymbol{A}^T\boldsymbol{A})^{-1}\boldsymbol{A}^T\boldsymbol{v} \quad (17)$$

5 Simulation and Results

In this section, the performance of the DNN as applied to the presented seismic model for DOA and position estimation algorithm are evaluated. The parameters used for WGs and WGNs deployment are listed in Table 1. Note that, these parameters are used for all evaluations unless otherwise stated.

5.1 Simulation Environment

The simulation parameters of the implemented DNN algorithm are presented in this section. A reference source i.e. WG is assumed to be transmitting a narrow band signal with 600 MHz carrier frequency. A 5-element ULA ($M = 5$) is used, where the inter-element spacing is $\lambda/2$ and $T = 100$ snapshots. The diagonal and lower triangular elements of correlation matrix are decomposed into a column vector, $\boldsymbol{q}$, of $M^2 = 25$ entries. This vector is used as an input to the DNN.

A feedforward neural network based on supervised learning algorithm trained with Levenberg Marquardt backpropagation algorithm (Trainlm) and gradient descent with momentum is used. Two hidden layers with a Sigmoid activation function and 20 neurons per layer is adopted, where a linear activation function is used at the output layer. Each input data has a desired target (output) for generating a weight that minimizes the error between actual and estimated output. The training data is generated using different SNR scenarios as:

a) Constant 0 dB SNR
b) Constant 5 dB SNR
c) Constant 30 dB SNR
d) 5 dB linear steps from 0 dB to 30 dB
e) 1 dB linear steps from 0 dB to 30 dB

Table 1. Parameter for deployment of WG and WGN

Parameter	Values
Number of RLs	30
Number of geophones per RL	480
Number of geophones per cell	~450
Spacing between RLs	200 m
Spacing between geophone in RL	25 m
Cell radius, R	1 km
Number of WGNs	36
Total number of geophones	14400
Total area of acquisition	72 $sq\ km$

The search range of the DOA at the output of DNN ranges from $-60°$ to $60°$ in steps of $1°$ resolution, yielding a total of $N_\theta = 121$ angles. A total of 1000 epochs are used to ensure convergence for validation/testing. While generating the training data, 300 Monte Carlo iterations are considered for each aforementioned SNR scenarios. This gives 36,300 train set for each constant case, 254,100 and 1,125,300 for 5-step and 1-step cases respectively. A total of 80% is used as training set and remaining 20% is used as validation set to avoid overfitting. For our tests, we used a PC with an Intel(R) Xeon(R) CPU E5-1620 v3 @ 3.5 GHz processor and 32 GB RAM.

5.2 Performance Evaluation of the DNN in DOA

The robustness of the proposed DNN algorithm is evaluated using root mean square error (RMSE) and the probability of estimating the correct DOA. The RMSE can be expressed as

$$\text{RMSE} = \sqrt{\frac{1}{NI}\sum_{n=1}^{N}\sum_{i=1}^{I}\left(\theta_i^{(n)} - \hat{\theta}_i^{(n)}\right)^2} \qquad (18)$$

where N is the number of Monte Carlo iterations, I is the number of WGs to be localized, $\theta_i^{(n)}$, and $\hat{\theta}_i^{(n)}$ are the actual and estimated DOA at n^{th} test for i^{th} WG. If the estimated angle is within $0.5°$ from the original angle, correct estimation is considered.

The probability of correct estimation and RMSE according to the aforementioned five SNR scenarios are presented in Fig. 6 and Fig. 7, respectively, with description of the SNR used for the training phase in the legend and testing phase in the abscissa. In general, the DNN trained with wider range SNR outperforms its counterparts trained with constant SNR, meaning that DNN trained at a constant SNR has good performance at that specific SNR and then performs poorly for other SNR values. Both the DNN trained with 1 dB and 5 dB step linear increased SNR have similar performance with RMSE of $0.3°$ at 0 dB. The probability of correct estimation is 87% at 0 dB SNR then it saturates to 100% at 8 dB SNR. There is minor advantage of 0.2 % in correct estimation when using 1 dB step compared with 5 dB step increase. Note that the best probability of correct estimation and the smallest RMSE are achieved at the trained SNR, beyond that the performances get worse due to the overfitting of the DNN. DNNs trained with a linear increased SNR achieve correct estimation at around 6 dB SNR, while MUSIC algorithm requires ~4 dB more, as illustrated in Fig. 6. On the other hand, the same DNNs realize lower RMSE at SNR < 9 dB compared with MUSIC algorithm as shown in Fig. 7. Beyond that, MUSIC algorithm performs better.

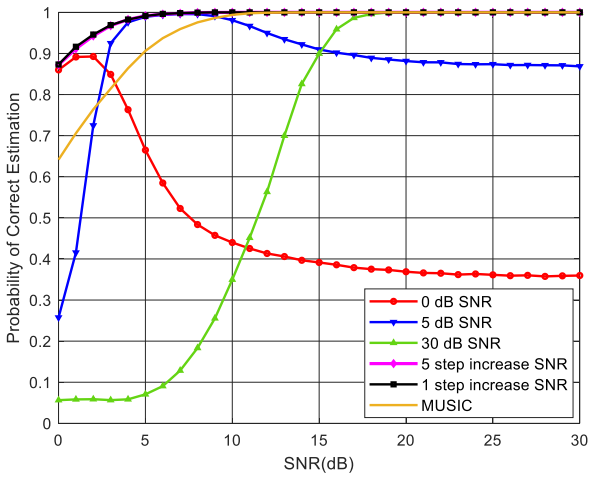

Fig. 6. Probability of correct DOA estimation for different training scenarios.

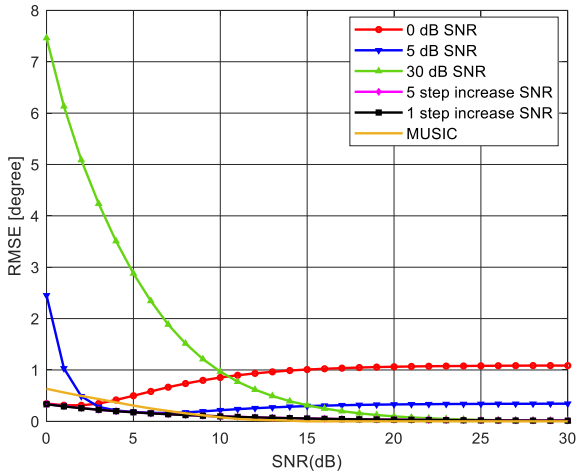

Fig. 7. RMSE of DOA estimation for each SNR scenario.

Table 2. Parameter for signal model

Parameter	Values
Centre frequency, f_c	600 MHz
No. of Snapshot, T	100
No. arrays element at each sector, M	5
Spacing between arrays, Δ	$\lambda/2$
Range covarage of arrays, N_θ	$121°$ ($-60°$ to $+60°$)
No. iteration, N	100
Initial transmitted power	40 dBm
Closest reference distance, d_0	1 m
Log-distance path loss exponent, n	2
Log-normal variance, σ^2	$0, 3, 5, 7$ dB

5.3 DOA Estimation Using DNN in Seismic Acquisition

In the previous subsection, the proposed DNN trained with a 1 step linear increase has a good performance in DOA estimations. This trained DNN is used in each sector of WGN for estimating the DOA of the received signals. The following discussion describes the effect of the channel model and the cell size on the estimation accuracy. The CDF of the MAE as a function of the position error is used to investigate the effect of path loss, where the position error is the Euclidian distance between the actual and the estimated position of the WGs. Then different shadowing effects were analyzed using the MAE and its empirical CDF as a function of the number of WGNs and position error, respectively. To investigate the effect of cell size, two different cell radii, $R = 1\ km$ and $R = 0.8\ km$, are examined in all cases. Note that, all parameters for generating the transmitted signal are given in Table 2. It is assumed that one WG is transmitting at a time and all WGs have equal transmitting power. The SNR of the received signal at the WGNs depends on path loss and the shadowing effects. Covariance matrices are formed from the received signal and applied to the DNN for DOA estimation. The results are then used for localization using the LSE.

The estimated DOA and the corresponding coordinates of WGNs are used in the LSE for estimating the position of the transmitter, i.e. WG, where the number of WGNs is determined as per the quality of the received signals. In other words, two or more of the nearest WGNs are used for estimating the position of one WG at a time. Accounting for more WGNs in LSE affects the estimation accuracy because the farther WGNs receive signals with a lower SNR, and this may bias the estimated location of the WG.

The MAE is defined as the mean of the Euclidian distance between the actual and the estimated position of the transmitting WG, which is given as

$$\text{MAE} = \frac{1}{NI}\sum_{n=1}^{N}\sum_{i=1}^{I}\sqrt{\left(X_{\text{WG}_i} - \hat{X}_{\text{WG}_i}^{(n)}\right)^2 + \left(Y_{\text{WG}_i} - \hat{Y}_{\text{WG}_i}^{(n)}\right)^2} \tag{19}$$

where $\hat{X}_{\text{WG}_i}^{(n)}$ and $\hat{Y}_{\text{WG}_i}^{(n)}$ are the estimated coordinates for the i^{th} WG at the n^{th} test. The localization based on DOA can be evaluated using different number of WGNs. We consider the strongest neighboring WGNs. Fig. 8 shows the empirical CDF of estimation accuracy as a function of the position error assessed using closest WGNs assuming no shadowing, $\sigma^2 = 0\ dB$. The localization accuracy increases with the number of WGNs because more WGNs are involved in the LSE. It also increases with reducing the cell radius, as the WGNs become closer to the WGs and consequently high SNR is realized at each WGN. For $R = 0.8\ km$ (dotted lines), four WGNs realize an excellent localization accuracy that is ~96% within $1.5\ m$ of the actual position. In the same vein, the accuracy is reduced by 2% or more in all considered cases when the cell radius is increased to $R = 1\ km$.

Fig. 9 shows the MAE in localizing all WGs versus the number WGNs involved in localization. Different shadowing levels are considered. In general, the MAE decreases with the number of considered WGNs until a certain value (4 WGNs) followed by a higher value due to the increase in the number of WGNs receiving the signal with a low SNR. For example, when $R = 1\ km$ and no shadowing i.e. $\sigma^2 = 0\ dB$, $4.4\ m$ MAE can be achieved using 2 WGNs. The accuracy increases to $0.6\ m$ using 4 WGNs, beyond which the performance deteriorates due to the aforementioned reason. Fig. 9 also shows that as the shadowing parameter, σ^2, increases, the localization accuracy decreases. When R is reduced to $R = 0.8\ km$, the MAE is further reduced.

Based on Fig. 9, a total of 4 WGNs is selected and the positioning accuracy using the empirical CDF of the MAE for all deployed WGs is plotted in Fig. 10 for different shadowing levels. The accuracy degrades as the shadowing parameter increases. When $R = 1\ km$ (solid lines), about 93.5% of the whole deployed WGs can be estimated within $1.5\ m$ of the actual position when only path loss effect is considered. When the shadowing level increases to $\sigma^2 = 7\ dB$ for the same cell size, about 65% of the whole deployed WGs is localized within $1.5\ m$ of the actual position. When the cell size is reduced, around 91% of the whole deployed WGs can be estimated within $1.5\ m$ of the actual position with shadowing level of $\sigma^2 = 3\ dB$.

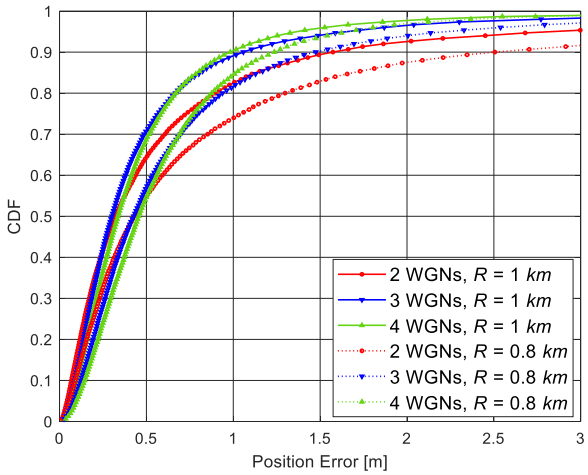

Fig. 8. Empirical CDF of localization error, evaluated using different cell radius and different number of WGNs.

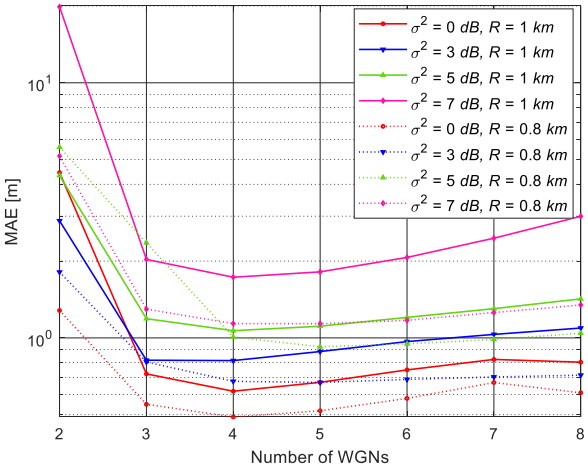

Fig. 9. Mean absolute error.

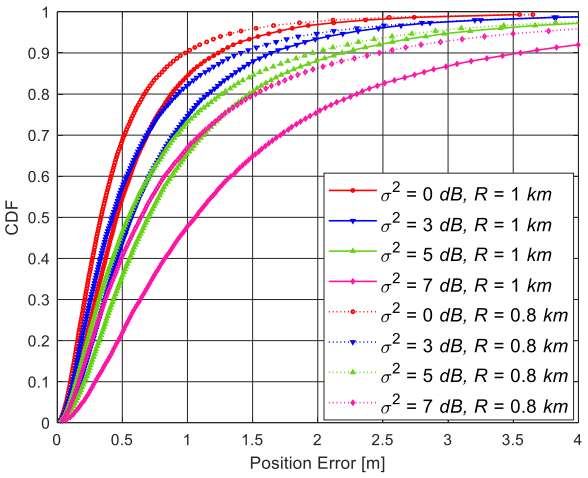

Fig. 10. Empirical CDF of localization error, evaluated using 4 WGNs, different cell radius and $\sigma^2 = 0, 3, 5, 7\ dB$.

6 Conclusion

This paper presented an orthogonal geometry of the wireless seismic model. The acquisition field was divided into hexagonal cells and each cell has a single WGN with three sectors. Also, a DOA estimation scheme was introduced based on DNN and its basic performance was tested using different SNR scenarios in the presence of one narrowband source. Simulation results show that a DNN trained with $1\ dB$ step SNR scenario achieves high DOA estimation accuracy. Moreover, the DNN DOA estimator was used in each sector of the WGN to estimate the DOA of the received signal. The estimated DOA and the corresponding coordinates of WGNs are used in LSE to estimate the position of the WGs. The result of position estimation depicts high estimation accuracy with the four closest WGNs. The estimation accuracy deteriorates as the shadowing effect increases and cell size increases. The results show that about 93.5% of the whole deployed WGs can be estimated within $1.5\ m$ of the actual position when only path loss effect is considered. When the shadowing level increases to $\sigma^2 = 7\ dB$, about 65% of the whole deployed WGs is localized within $1.5\ m$ of the actual position for the same cell size, $R = 1\ km$.

References

[1] R. Khan and S. A. Zummo, "Functional Quantization-Based Data Compression in Seismic," *Arab. J. Sci. Eng.*, vol. 44, no. 3, pp. 2151–2163, 2019.

[2] H. H. Nuha, A. Balghonaim, B. Liu, and M. Mohandes, "Deep Neural Networks with Extreme Learning Machine for Seismic Data Compression," *Arab. J. Sci. Eng.*, vol. 45, no. 3, pp. 1367–1377, 2020.

[3] S. Savazzi, U. Spagnolini, L. Goratti, D. Molteni, M. Latva-Aho, and M. Nicoli, "Ultra-Wide Band Sensor Networks in Oil and Gas Explorations," *IEEE Commun. Mag.*, vol. 51, no. 4, pp. 150–160, Apr. 2013.

[4] V. A. Reddy, G. L. Stuber, S. Al-Dharrab, W. Mesbah, and A. H. Muqaibel, "Energy-Efficient mm-Wave Backhauling via Frame Aggregation in Wide Area Networks," *IEEE Trans. Wirel. Commun.*, 2021.

[5] A. Mahmood, R. Exel, H. Trsek, and T. Sauter, "Clock Synchronization Over IEEE 802.11 - A Survey of Methodologies and Protocols," *IEEE Trans. Ind. Informatics*, vol. 13, no. 2, pp. 907–922, 2017.

[6] Q. Liu, Y. Gu, and H. C. So, "DOA Estimation in Impulsive Noise via Low-Rank Matrix Approximation and Weakly Convex Optimization," *IEEE Trans. Aerosp. Electron. Syst.*, vol. 55, no. 6, pp. 3603–3616, 2019.

[7] H. Cao, Q. Liu, and Y. Wu, "Transform Domain: Design of Closed-Form Joint 2-D DOA Estimation Based on QR Decomposition," *Circuits, Syst. Signal Process.*, vol. 39, no. 10, pp. 5318–5329, 2020.

[8] Q. Liu, H. C. So, and Y. Gu, "Off-Grid DOA Estimation with Nonconvex Regularization via Joint Sparse Representation," *Signal Processing*, vol. 140, pp. 171–176, 2017.

[9] J. Tian, M. Gao, and H. Zhou, "Multi-channel Seismic Data Synchronizing Acquisition System based on Wireless Sensor Network," in *2008 IEEE International Conference on Networking, Sensing and Control, Sanya, China*, 2008, pp. 1269–1272.

[10] A. D. L. M. Pellegrino, N. Pajola, G. Tortini, A. Esposito, P. Follino, "Wireless vs Wireline Land 3D Seismic in North Italy," in *SEG Technical Program Expanded Abstracts*, 2012, pp. 1–5.

[11] S. Savazzi and U. Spagnolini, "Wireless Geophone Networks for High-Density Land Acquisition: Technologies and Future Potential," *Lead. Edge*, vol. 27, no. 7, pp. 882–886, Jul. 2008.

[12] S. Savazzi and U. Spagnolin, "Synchronous Ultra-wide Band Wireless Sensors Networks for Oil and Gas Exploration," in *2009 IEEE Symposium on Computers and Communications, Sousse, Tunisia*, 2009, pp. 907–912.

[13] S. Savazzi, L. Goratti, D. Fontanella, M. Nicoli, and U. Spagnolini, "Pervasive UWB Sensor Networks for Oil Exploration," in *Proceedings - IEEE International Conference on Ultra-Wideband (ICUWB), Bologna, Italy*, 2011, pp. 225–229.

[14] V. A. Reddy, G. L. Stueber, and S. I. Al-Dharrab, "Energy Efficient Network Architecture for Seismic Data Acquisition via Wireless Geophones," in *IEEE International Conference on Communications, Kansas, USA*, 2018, vol. 2018-May, pp. 1–5.

[15] S. Qiao *et al.*, "Development of high-precision distributed wireless microseismic acquisition stations," *Geosci. Instrumentation, Methods Gata Syst.*, vol. 7, no. 3, pp. 253–263, 2018.

[16] I. W. Sudiarta, R. F. Akmaludin, D. W. Kurniawidi, and M. S. Yadnya, "Wireless System for Active Seismic Method," in *2016 International Symposium on Electronics and Smart Devices, ISESD Bandung, Indonesia*, 2017, pp. 85–87.

[17] F. Foroozan, A. Asif, and Y. Jin, "Direction Finding Algorithms for Time Reversal MIMO RADARs," *IEEE Stat. Signal Process. Work. (SSP), Nice, Fr.*, pp. 433–436, Jun. 2011.

[18] S. A. Alawsh, A. H. Muqaibel, and M. S. Sharawi, "Sparse Direction-of-Arrival Estimation for Two Sources with Constrained Antenna Arrays," in *10th International Conference on Electrical and Electronics Engineering, Bursa, Turkey*, 2017, pp. 666–670.

[19] G. Pan, L. Fu, Q. Chen, M. Yu, and M. Muresan, "Road Safety Performance Function Analysis with visual Feature Importance of Deep Neural Nets," *IEEE/CAA J. Autom. Sin.*, vol. 7, no. 3, pp. 735–744, 2020.

[20] P. M. Kebria, A. Khosravi, S. M. Salaken, and S. Nahavandi, "Deep Imitation Learning for Autonomous Vehicles based on Convolutional Neural Networks," *IEEE/CAA J. Autom. Sin.*, vol. 7, no. 1, pp. 82–95, 2020.

[21] Z. Huang, X. Xu, H. Zhu, and M. C. Zhou, "An Efficient Group Recommendation Model with Multiattention-Based Neural Networks," *IEEE Trans. Neural Networks Learn. Syst.*, vol. 31, no. 11, pp. 4461–4474, 2020.

[22] M. F. Unlersen and E. Yaldiz, "Direction of Arrival Estimation by Using Artificial Neural Networks," in *2016 European Modelling Symposium (EMS), Pisa, Italy*, 2016, pp. 242–245.

[23] Y. Kase, T. Nishimura, T. Ohgane, Y. Ogawa, D. Kitayama, and Y. Kishiyama, "DOA Estimation of Two Targets with Deep Learning," in *2018 15th Workshop on Positioning, Navigation and Communications, WPNC 2018, Bremen, Germany*, 2018, no. 2, pp. 1–5.

[24] Z. M. Liu, C. Zhang, and P. S. Yu, "Direction-of-Arrival Estimation Based on Deep Neural Networks with Robustness to Array Imperfections," *IEEE Trans. Antennas Propag.*, vol. 66, no. 12, pp. 7315–7327, Dec. 2018.

[25] S. Abeywickrama, L. Jayasinghe, H. Fu, S. Nissanka, and C. Yuen, "RF-based Direction Finding of UAVs Using DNN," in *2018 IEEE International Conference on Communication Systems, ICCS 2018, Chengdu, China*, 2018, pp. 157–161.

[26] H. Huang, J. Yang, H. Huang, Y. Song, and G. Gui, "Deep Learning

for Super-resolution Channel Estimation and DOA Estimation Based Massive MIMO System," *IEEE Trans. Veh. Technol.*, vol. 67, no. 9, pp. 8549–8560, Sep. 2018.

[27] H. Huang, G. Gui, H. Sari, and F. Adachi, "Deep Learning for Super-Resolution DOA Estimation in Massive MIMO Systems," in *2018 IEEE 88th Vehicular Technology Conference (VTC-Fall), Chicago, USA*, 2018, vol. 2018-Augus, pp. 1–5.

[28] S. Chakrabarty, S. Member, A. P. Habets, and S. Member, "Multi-Speaker DOA Estimation Using Deep Convolutional Networks Trained With Noise Signals," *IEEE J. Sel. Top. Signal Process.*, vol. 13, no. 1, pp. 8–21, Mar. 2019.

[29] K. Doğançay, "Bearings-only Target Localization Using Total Least Squares," *Signal Processing*, vol. 85, no. 9, pp. 1695–1710, Sep. 2005.

[30] A. H. Sayed, A. Tarighat, and N. Khajehnouri, "Network-based Wireless Location: Challenges Faced in Developing Techniques for Accurate Wireless Location Information," *IEEE Signal Process. Mag.*, vol. 22, no. 4, pp. 24–40, Jul. 2005.

[31] A. Almehdhar *et al.*, "DOA Estimation in Wireless Seismic Surveys Using Deep Learning," *Int. Conf. Commun. Signal Process. their Appl. (ICCSPA), Sharjah, United Arab Emirates*, pp. 1–6, 2021.

[32] T. O. Olasupo, C. E. Otero, K. O. Olasupo, and I. Kostanic, "Empirical Path Loss Models for Wireless Sensor Network Deployments in Short and Tall Natural Grass Environments," *IEEE Trans. Antennas Propag.*, vol. 64, no. 9, pp. 4012–4021, Sep. 2016.

[33] A. Alsayyari, I. Kostanic, C. Otero, M. Almeer, and K. Rukieh, "An empirical path loss model for wireless sensor network deployment in a sand terrain environment," in *2014 IEEE World Forum on Internet of Things, WF-IoT 2014, Seoul, Korea*, 2014, pp. 218–223.

[34] J. Miranda *et al.*, "Path loss exponent analysis in Wireless Sensor Networks: Experimental evaluation," in *IEEE International Conference on Industrial Informatics (INDIN), Bochum, Germany*, 2013, no. July, pp. 54–58.

[35] Y. S. Erogluy, I. Guvency, N. Palay, and M. Yukselz, "AOA-Based Localization and Tracking in Multi-Element VLC Systems," in *2015 IEEE 16th Annual Wireless and Microwave Technology Conference, WAMICON 2015, Florida, USA*, 2015, pp. 1–5.

Author Contributions

Conceptualization, A.M., W.M, and G.S; methodology, K.A, A.M., V.R., and A.B.; validation, K.A and S.A.; data curation, K.A and S.A.; Analysis, A.M., S.A., W.M, V.R., A.B., and G.S; writing—original draft preparation, K.A, S.A., and A.M.; project administration and funding acquisition, A.M and S.A. All authors have read and agreed to the published version of the manuscript.

Competing interests

The authors declare no competing interests.